A comparison of Hartree–Fock and exact diagonalization solutions for a model two-electron system

David C. Thompson and Ali Alavi

Citation: J. Chem. Phys. **122**, 124107 (2005); doi: 10.1063/1.1869978
View online: http://dx.doi.org/10.1063/1.1869978
View Table of Contents: http://aip.scitation.org/toc/jcp/122/12
Published by the American Institute of Physics

A comparison of Hartree–Fock and exact diagonalization solutions for a model two-electron system

David C. Thompson[a] and Ali Alavi
Cambridge University Centre for Computational Chemistry, Lensfield Road, Cambridge CB2 1EW, United Kingdom

(Received 19 August 2004; accepted 20 January 2005; published online 29 March 2005)

We compare the restricted (RHF) and unrestricted (UHF) Hartree–Fock solutions with the exact configuration interaction (CI) solutions for the model problem of two interacting electrons confined within an infinite spherical potential of radius R. An investigation of the ground state energy, electron density, and a population analysis of the wave functions reveals that the UHF solution compares favorably with the CI one in both the small and large R limits. The Coulson–Fischer transition (the point at which the RHF and UHF solutions are no longer degenerate) occurs at an $r_s \equiv R/2^{1/3} \approx 6$ a.u., close to the crossover r_s where the exact CI density acquires a minimum at the sphere center; this behavior captures the onset of Wigner molecule formation. In this regime, however, the HF densities and energies are not quantitatively accurate when compared to the CI ones. This failure is further quantified by computing E_c/E to determine the ability of each method at capturing the exact correlation energy; we conclude that the UHF solutions can be reasonably accurate at both high and low densities, but not at intermediate r_s. © *2005 American Institute of Physics*. [DOI: 10.1063/1.1869978]

I. INTRODUCTION

The use of exact solutions of model problems to test commonly used theoretical approaches is not new. A system that has drawn considerable attention over a number of years is that of "Harmonium" or the Hooke's law atom. This model problem consists of two electrons in an external harmonic oscillator potential and was shown to be analytically solvable for a denumerable infinite set of oscillator frequencies.[1,2] This system is of interest for numerous reasons. First, the strength of the interaction, i.e., the magnitude of the spring constant ω governing the strength of the harmonic potential, can be used to take the system from being weakly correlated (large ω) to strongly correlated (small ω). Second, the model contains a realistic Coulombic interaction between the particles—the study of which is vital to an understanding of many-body phenomena in physics.

The exact solutions arising from this problem have been used to test commonly used density functionals; the ability to tune the correlation between the particles through variation of ω admits for testing of these approximations in very different regimes of physical interest.[3–5] Also, recently, work has been aimed at using this model system to better understand the *exact* exchange-correlation functional.[6,7]

The model system discussed in this work, that of two interacting electrons confined through an infinite spherical potential of radius R, has been recently solved using configuration interaction (CI) methods.[8,9] Analogous to the strength of the harmonic potential in Harmonium, the physical extent of a confining potential is directly proportional to the effective Coulomb coupling between the particles. The correlation in this system has both dynamical and nondynamical character, depending on the sphere size. For small spheres, the CI wave function is dominated by one Slater determinant, with many very small contributions arising from excited-state Slater determinants. This behavior is characteristic of dynamical correlation. In the large-sphere limit, the CI expansion becomes multiconfigurational. Although the density remains spherically symmetric, it becomes depleted in the center of the sphere, and develops an increasingly pronounced maximum off-center. The character of this regime is best studied via the pair-correlation function of the two electrons, which acquires a strongly peaked structure at a distance remote from the reference electron. This limit is referred to as a Wigner molecule limit, in analogy with the Wigner crystallization of the uniform electron gas,[10] in which the electrons localize at the sites of a regular bcc crystal in order to minimize their mutual Coloumb repulsion. The intermediate regime, which corresponds to the crossover between the small-sphere and large-sphere limits is particularly interesting. Here, the wave function has simultaneously both dynamical and nondynamical character. The purpose of this paper is to examine the performance of mean-field approaches (primarily Hartree–Fock at the restricted and unrestricted levels) in describing this system over a broad range of sphere sizes. We compare these solutions to the CI ones and present a detailed analysis to determine how, and hypothesize why, these mean-field solutions differ from the exact CI ones.

This work is organized in the following way: In Sec. II we formally introduce the problem and method of solution using both the restricted (RHF) and unrestricted Hartree–Fock (UHF) methodologies. In Sec. III to validate the use of

[a]Author to whom correspondence should be addressed. Present address: Department of Chemistry, McMaster University, 1280 Main St. West, Hamilton, ON, Canada. Electronic mail: thompda@mcmaster.ca

our code we compute confined atomic hydrogen, helium, and beryllium solutions at the RHF level and compare to existing studies. In Sec. IV we compute the RHF and UHF solutions for the model problem at hand and compare to the exact CI solutions; we shall consider the total ground state energy, the electron density, and a population analysis of the corresponding wave functions. Section V will contain concluding remarks.

II. MODEL PROBLEM AND HARTREE–FOCK METHODOLOGY

The two-electron Hamiltonian for the problem (Hartree atomic units $\hbar = m_e = e^2 = 1$ are used throughout) is written as

$$\hat{H} = \hat{T} + \hat{U} + \hat{V}, \tag{1}$$

$$\hat{T} = -\frac{1}{2}\sum_{i=1}^{2} \nabla_i^2, \tag{2}$$

$$\hat{U} = \frac{1}{|\mathbf{r}_1 - \mathbf{r}_2|}, \tag{3}$$

$$\hat{V} = \sum_{i=1}^{2} v_{\text{ext}}(\mathbf{r}_i). \tag{4}$$

Here we define the external potential to be

$$v_{\text{ext}}(\mathbf{r}) = \begin{cases} 0, & r < R \\ \infty, & r \geqslant R. \end{cases} \tag{5}$$

In general the Hartree–Fock equations are solved to find a set of spin orbitals χ such that a Slater determinant formed from these orbitals is the best single determinantal approximation to the ground state of the system, in this work we shall consider both restricted and unrestrcited solutions to the Hartree–Fock equations.

A. Restricted Hartree–Fock

For the problem of interest, in the closed-shell RHF formalism, both electrons are paired and occupy a single spatial orbital such that the corresponding determinant becomes

$$|\psi_{\text{RHF}}\rangle = \psi_1(\mathbf{r}_1)\psi_1(\mathbf{r}_2)\frac{1}{\sqrt{2}}[\alpha_1\beta_2 - \beta_1\alpha_2], \tag{6}$$

with ψ and α/β denoting spatial and spin orbitals, respectively [with Eq. (6) resulting in the $S=0$ solution]. The canonical HF equations written in this form can be solved following Roothaan[11] where the HF orbital is expanded in a set of known spatial basis functions. Given that, for this two-electron system of interest, the RHF wave function is an eigenfunction of the S^2 operator, and given that we know the exact ground state to the fully interacting problem has a ^1S term symbol,[8,9] the RHF orbitals can be well represented through spherically symmetric basis functions. A natural choice for such functions are the zeroth-order spherical Bessel functions, such that

$$\psi_1(\mathbf{r}) = \frac{1}{\sqrt{4\pi}}\sum_{\mu=1}^{\mu_{\max}} C_{\mu 1} N_{\mu 0} j_0(\alpha_{\mu 0} r), \tag{7}$$

where $N_{\mu 0}$ are appropriate normalization constants

$$N_{\mu 0} = \sqrt{\frac{2}{R^3}}\frac{\mu\pi}{(-)^{\mu+1}} \tag{8}$$

and

$$j_0(r) = \frac{\sin(r)}{r}. \tag{9}$$

The $\alpha_{\mu 0}$ are the roots of the zeroth-order spherical Bessel functions needed to satisfy the condition that the wave function vanish at the boundary of the sphere, $\alpha_{\mu 0} = \mu\pi/R$. The matrix representation of the Fock operator is written as

$$F_{\mu\nu} = T_{\mu\nu} + v_{\mu\nu}^{\text{ext}} + G_{\mu\nu} \equiv H_{\mu\nu} + G_{\mu\nu}, \tag{10}$$

where $H_{\mu\nu}$ is a sum of one-electron terms which do not change at all during the course of a calculation. The **G** matrix contains the two-electron components of the system and its contribution changes throughout the iterative process. We shall now discuss the analytic form of each of these matrix elements.

In a basis of zeroth-order spherical Bessel functions, the kinetic energy term is diagonal

$$T_{\mu\nu} = \delta_{\mu\nu}\frac{\alpha_{\mu\nu}^2}{2} = \delta_{\mu\nu}\frac{\mu^2\pi^2}{2R^2}. \tag{11}$$

In order to validate the implementation of the code, we consider an external potential

$$v_{\text{ext}}(\mathbf{r}) = \begin{cases} -\dfrac{Z_{\text{nucl}}}{r}, & r \leqslant R \\ \infty, & r > R. \end{cases} \tag{12}$$

The use of this term enables us to calculate "confined atomic" systems. The matrix elements, involving this potential, in our choice of basis functions can be shown to be analytic,

$$\begin{aligned} v_{\mu\nu}^{\text{ext}} &= -\frac{Z_{\text{nucl}}}{R}[\gamma - \text{Ci}(2\pi\mu) + \ln(2\pi\mu)], \quad \mu = \nu \\ &= \frac{Z_{\text{nucl}}}{R}\frac{1}{(-)^{\mu+\nu+1}}\Bigg\{\text{Ci}[(\mu-\nu)\pi\,\text{Sgn}(\mu-\nu)] \\ &\quad - \text{Ci}[(\mu+\nu)\pi] + \ln\left(\frac{\mu+\nu}{\mu-\nu}\right)\Bigg\}, \quad \mu \neq \nu. \end{aligned} \tag{13}$$

Here, γ is Euler's constant and the Ci's are cosine integrals evaluated using a standard numerical method.[12] With $Z_{\text{nucl}} = 0$ we recover the v_{ext} of Eq. (5).

The **G** matrix can be decomposed into primitive direct and exchange Coulomb integrals

$$G_{\mu\nu} = \sum_{\mu\nu} P_{\mu\nu}[2\langle\mu\sigma|\nu\lambda\rangle - \langle\mu\sigma|\lambda\nu\rangle], \tag{14}$$

where

$$P_{\mu\nu} = C^*_{\mu 1} C_{\nu 1} \tag{15}$$

defines a density matrix **P**. The primitive Coulomb integrals in a basis of zeroth-order spherical Bessel functions are analytic and have been discussed in Ref. 8.

B. Closed-shell unrestricted Hartree–Fock

In the closed-shell UHF formalism the usual RHF wave function is generalized to allow the α and β electrons to occupy different spatial orbitals. These orbitals take the form

$$\chi_1(\mathbf{x}) = \begin{cases} \psi_1^{\alpha}(\mathbf{r})\alpha(\sigma) \\ \psi_1^{\beta}(\mathbf{r})\beta(\sigma) \end{cases}, \tag{16}$$

such that the RHF restriction $\psi_1^{\alpha} \equiv \psi_1^{\beta} \equiv \psi_1$ has been removed. The Fock operators associated with this more general approach contain mixed terms; an operator for the alpha electron sees a self-interaction free potential and a Coulomb potential due to the β electron. Expanding the UHF orbitals in a suitable spatial basis we form the Pople–Nesbet matrix equations[13] and solve these equations self-consistently. The UHF wave function suffers from the disadvantage that it is not an eigenfunction of the S^2 operator; the total spin angular momentum is not a well defined quantity. Thus, the appropriate basis for the UHF study will be

$$\psi_1(\mathbf{r}) = \sum_{\mathbf{n}}^{\mu_{\max}, l_{\max}} C_{\mathbf{n}1}\, \eta_{\mathbf{n}}(\mathbf{r}), \tag{17}$$

where now, $\mathbf{n} = (\mu l m)$ is a three-vector of quantum numbers and $\eta_{\mathbf{n}}(\mathbf{r}) = N_{\mu l} j_l(\alpha_{\mu l} r) Y_{lm}(\theta, \phi)$ are eigenfunctions of the one-electron Schrödinger equation in a hard-spherical cavity, with $\alpha_{\mu l}$ choosen so that the radial boundary condition $j_l(\alpha_{\mu l} R) = 0$ is met, i.e., $\alpha_{\mu l} R = k_{\mu l}$ is the μth root of the lth spherical Bessel function. $\mu_{\max}$ and $l_{\max}$ refer to the maximum principal μ and angular momentum l quantum number which defines the size of the basis. The $N_{\mu l}$ are normalization constants such that

$$N_{\mu l} = \sqrt{\frac{2}{R^3}} [j_{l+1}(k_{\mu l})]^{-1}. \tag{18}$$

We find that the kinetic energy is diagonal in this basis:

$$T_{\mathbf{n}\mathbf{n}'} = \delta_{\mathbf{n}\mathbf{n}'} \frac{k_{\mu l}^2}{2R^2}. \tag{19}$$

Also, those primitive Coulomb integrals containing nonzero total angular momentum are no longer analytic and their numerical evaluation has been discussed, at length, in Refs. 8 and 9.

C. Self-consistent-field methodology

We briefly detail here the specifics of our self-consistent-field algorithm implementation.

(1) We guess an initial density matrix. We have tried $\mathbf{P}^{\text{initial}} = \mathbf{0}$, slightly randomized, and constructed from HF orbitals from prior calculations. Special care is taken in solving the Pople–Nesbet equations when $N^{\alpha} = N^{\beta}$. In this instance, starting with $\mathbf{P}^{\alpha}_{\text{initial}} = \mathbf{P}^{\beta}_{\text{initial}}$, we would recover the *restricted* solution to the Roothaan equations. In addition to this solution there exists an energetically lower unrestricted solution corresponding to $\mathbf{P}^{\alpha}_{\text{initial}} \neq \mathbf{P}^{\beta}_{\text{initial}}$. We have made sure that we have obtained the UHF solutions wherever quoted.

(2) Calculate the **G** matrix. Before beginning the self-consistent-field (SCF) iterations all possible combinations of $\langle \mu\sigma | \nu\lambda \rangle$ are calculated. We employ symmetries that exist between interchange of μ, ν, λ, and σ and the elements are stored during an initialization step. **G** is then formed at each step from the primitives held in memory and the density matrix for that iteration.

(3) We add **H** to **G** to form **F**.

(4) We diagonalize **F** to find the eigenvalues ϵ and eigenvectors **C**. The diagonalization is performed using DSYEVX (Ref. 14) a LAPACK routine used for diagonalizing real, symmetric matrices.

(5) Form $\mathbf{P}^{\text{new}}$ from **C** and check convergence.

(6) If the convergence is within user specified tolerance we finish the calculation and determine useful properties. Else go to step (2). Following Ref. 15 we define our convergence with respect to the standard deviation of the ith and $(i-1)$th density matrices. We have chosen our convergence criteria δ to be 10^{-10}.

III. CONFINED ATOMIC SYSTEMS

There is great interest in the field of confined atomic and molecular species. Although somewhat exotic, this branch of study is found to have important implications to such diverse fields as condensed matter and astrophysics.[16,17] The study of confined atomic systems began with the work of Michels, De Boer, and Bijl who first considered the problem of confined atomic hydrogen.[18] Several years later, Ten Seldam and De Groot[19,20] looked at the compressibility of confined atomic helium. Recently work has been performed on hydrogen, helium, and other simple first row atoms, confined through either penetrable or impenetrable walls of differing geometries.[21–23]

As we will be using these systems to validate our sought after solutions to our model problem, it is a pertinent question to ask at the outset how good a basis of zeroth-order spherical Bessel functions is at reproducing atomic wave functions? In order to address this question, we consider a Fourier–Bessel[24] expansion of the exponential function $e^{-\alpha r}$:

$$\exp(-\alpha r) = \lim_{\mu_{\max} \to \infty} \frac{1}{\sqrt{4\pi}} \sum_{\mu}^{\mu_{\max}} B_{\mu} N_{\mu 0} j_0(\alpha_{\mu 0} r). \tag{20}$$

We can solve for B_{μ} in the above expression and find that

$$\frac{B_{\mu}}{\sqrt{4\pi}} = N_{\mu 0} \left[\frac{2\alpha}{\alpha^2 + \alpha_{\mu 0}^2} - \frac{\exp(-\alpha R)(-)^{\mu}}{\alpha^2 + \alpha_{\mu 0}^2} \times \left(R + \frac{2\alpha}{\alpha^2 + \alpha_{\mu 0}^2} \right) \right]. \tag{21}$$

Figure 1 illustrates how slowly convergent a spherical Bessel representation of the exponential is; we expect from this analysis that a large number of basis functions will need to be included in the expansions to correctly describe the system. The poor description of the function at the end points is a function of R. To better illustrate this dependence upon R,

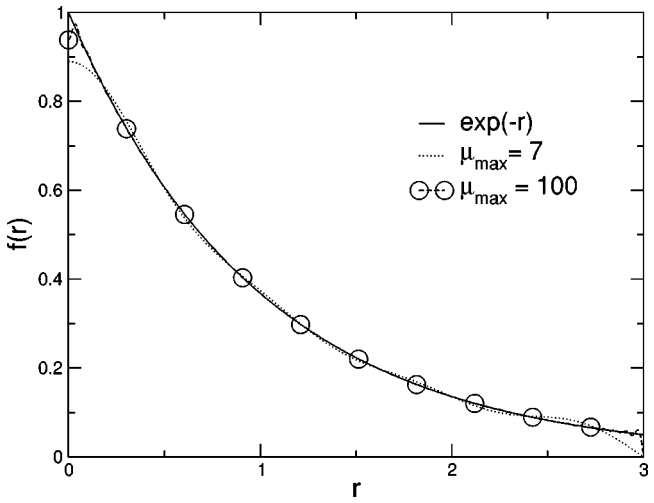

FIG. 1. An expansion of an exponential function $e^{-\alpha r}$ using spherical Bessel functions of the zeroth-order [Eq. (7)], using the coefficients as determined through Eq. (21). Here $\alpha=1$ and $R=3$. $\mu_{\max}$ is defined through Eq. (18).

Fig. 2 shows the rate of convergence of the helium RHF energy as a function of the number of basis functions $\mu_{\max}$ used in Eq. (7). For the unit sphere we are simply unable to represent the correct form of the wave function and this results in an incorrect, unphysical, solution. The fastest convergence is observed for $R=5$, and for the larger spheres it appears as if the more oscillatory functions, of larger radial extent, are needed to correctly model this helium system.

In Table I we show the RHF hydrogen, helium, and beryllium energies computed using a spherical Bessel expansion. It will be noted that we have also performed local density approximation (LDA) functional calculations for the helium system. An LDA calculation requires evaluation of one-electron integrals of the type

$$v_{\mu\nu}^{\mathrm{xc}} = \int d\mathbf{r}\phi_{\mu}^{*}(\mathbf{r})v_{\mathrm{xc}}(\mathbf{r})\phi_{\nu}(\mathbf{r}), \tag{22}$$

where v_{xc} is explicitly linked to the form of the exchange-correlation energy functional used, and ϕ_{μ} are Kohn–Sham

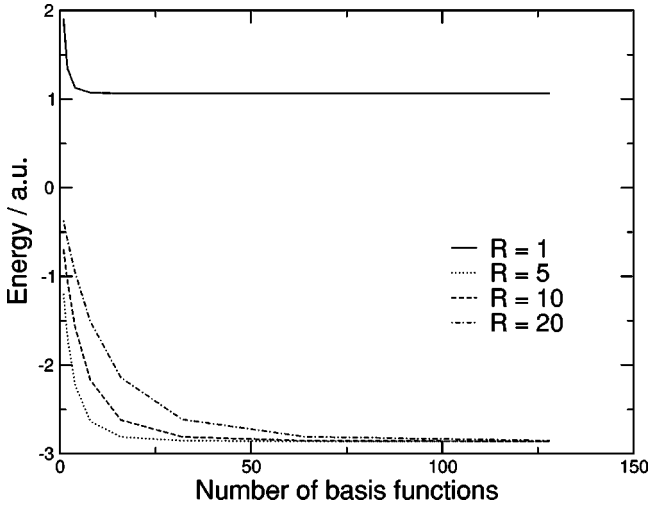

FIG. 2. The convergence of the ground state confined helium RHF energy as a function of number of basis functions, shown for $R=1$, 5, 10, and 20. Fastest convergence is observed for $R=5$.

TABLE I. RHF energy convergence as a function of basis set size, $R=5$. Also shown is the LDA energy of the helium system. For this calculation $R=5$ and we have used the Perdew–Zunger parametrization of ϵ_c (Ref. 25). For comparison we include RHF and LDA calculations from Refs. 28 and 29, respectively; these are the last entries in the table.

$\mu_{\max}$	Hydrogen[a]	Helium[a]	Beryllium[a]	Helium[b]
1	−0.194 42	−0.697 76		−1.223 62
4	−0.377 91	−1.569 00	−4.817 676	−2.214 11
8	−0.457 78	−2.170 19	−7.617 451	−2.610 84
16	−0.491 02	−2.620 86	−10.880 78	−2.784 37
32	−0.498 59	−2.809 78	−13.319 97	−2.825 90
64	−0.499 81	−2.853 58	−14.310 25	−2.832 63
80	−0.499 90	−2.857 38	−14.425 83	−2.833 14
128	−0.499 97	−2.860 58	−14.532 52	−2.833 56
	−0.5	−2.8617	−14.5730	−2.8254

[a]RHF energy convergence as a function of basis set size, $R=5$.
[b]Also shown is the LDA energy of the helium system.

orbitals. In evaluating these elements 500 radial mesh points were used with the Slater–Dirac exchange and the local density correlation functional of Perdew and Zunger (PZ).[25]

IV. TWO INTERACTING ELECTRONS

We turn now to the object of this present study. Setting $Z_{\mathrm{nucl}}=0$ allows us to determine the RHF energy of this model problem as a function of R. In Table II we present the convergence of the RHF energy of this two-electron system.

TABLE II. RHF energy convergence as a function of sphere size. Relative differences are with respect to the largest basis set used. Relative errors are with respect to the exact CI energy. The agreement for small R is reasonable but is seen to worsen, markedly, for increasing R.

Radius of sphere	r_s (a.u.)	$\mu_{\max}$	Energy (a.u.)	Relative difference
1	0.79	1	11.655 677 574	1×10^{-2}
		2	11.641 762 164	1×10^{-5}
		3	11.641 749 013	1×10^{-6}
		4	11.641 747 907	3×10^{-7}
		5	11.641 747 705	6×10^{-8}
		6	11.641 747 658	1×10^{-8}
		7	11.641 747 645	
Exact			11.5910	0.437%
5	3.97	1	0.751 998 811	1×10^{-2}
		2	0.739 872 477	1×10^{-4}
		3	0.739 764 754	3×10^{-6}
		4	0.739 762 197	4×10^{-7}
		5	0.739 761 893	9×10^{-8}
		6	0.739 761 826	2×10^{-8}
		7	0.739 761 807	
			0.7016	5.440%
20	15.87	1	0.113 977 670	9×10^{-3}
		2	0.105 786 504	4×10^{-4}
		3	0.105 399 305	2×10^{-5}
		4	0.105 380 112	2×10^{-6}
		5	0.105 378 745	2×10^{-7}
		6	0.105 378 556	5×10^{-8}
		7	0.105 378 511	
			0.0866	21.71%

TABLE III. Presented below are the LDA energies for the PZ functional (Ref. 25). The energies are computed with $\mu_{max}=7$. Relative errors are computed using the exact energy as determined through CI.

Radius of sphere	r_s (a.u.)	PZ Energy (a.u.)	Relative error
1	0.79	11.734 843 308	1.24%
5	3.97	0.709 864 982	1.19%
20	15.87	0.082 471 698	−4.73%

Using only seven basis functions we obtain excellent levels of convergence, even for large spheres. The increased rate of convergence of this study as compared to the confined atomic systems is understood simply if we consider that we are now trying to represent a wave function with spherical Bessel character through spherical Bessel functions; clearly a rapidly convergent expansion. We also compute the LDA energy using the PZ correlation functional with Slater exchange (Table III), for small (=1) and large (=20) R, the LDA, approximation does not satisfactorily model this system. This has been remarked in the work of Jung *et al.* who also show that in general the LDA behaves poorly. This, they attribute to a systematic underestimation of the exchange energy.[26] We will later compare the densities.

In Table IV we present the UHF energies as a function of the μ_{max} and l_{max} quantum numbers. We find that the $\mu_{max}=3$, $l_{max}=4$ basis set containing 75 basis functions, provides a good representation of the system for all R considered. We have included both the low- and high-spin UHF states, with $m_s=0$ and $m_s=1$, respectively. These correspond to the ^1S and first excited ^3P states found in the CI solution. Upon comparison with Table I we find that for $R>5$, $E_{UHF}<E_{RHF}$, and we have passed through what may be described as a "Coulson–Fischer" transition:[27] the extra freedom afforded to the UHF solution—namely, the ability to separate the spatial distribution of the α and β spins—leads to a lowering of energy, which grows with increasing R. To further highlight this, below in Fig. 3, we show the energy of a number of different states at both the RHF, UHF, and CI levels of theory. In general a scaled energy plot (Er_s^2 vs r_s, where r_s represents the Wigner–Seitz radius and is given by $R/2^{1/3}$) will appear linear as we know that a reasonable approximation to the energy is given by $Er_s^2 \sim Ar_s+B+\ldots$. This follows from transforming the Hamiltonian into scaled units using r_s; we see that the kinetic and Coulombic components scale as $\approx 1/r_s^2$ and $\approx 1/r_s$, respectively. For small r_s (kinetic energy regime) the HF solutions to both the ^1S and ^3P states are in reasonable agreement with the exact CI energies: $[E^{UHF}_{1\alpha 1\beta}(R=1)=11.642,\ E^{Cl}_{1S}(R=1)=11.591;\ E^{UHF}_{2\alpha}(R=1)=16.282,\ E^{Cl}_{^3P}(R=1)=16.277]$. This agreement is seen to lessen for increasing R. We see that the restricted and low-spin unrestricted solutions are degenerate until $r_s\approx 6$, with the UHF energy subsequently becoming lower in energy for increasing R. The Coulson–Fischer transition is evident. For large R, where now we are in a Coulomb dominant region, the ^1S and ^3P energies (scaled by r_s^2) differ by an almost constant amount. This implies that the singlet-triplet separation goes as r_s^{-2} in the large r_s limit. The separation between the low-spin ($\alpha\beta$) and high-spin ($\alpha\alpha/\beta\beta$) UHF energies, however, decay much more rapidly, becoming essentially degenerate at $r_s\approx 20$. The relative accuracies of the RHF and UHF solutions can be assessed through the function $|E_c/E|$, where $E_c=E_{Cl}-E_{RHF/UHF}$ (i.e., defined either with respect to the RHF or UHF solutions), shown in Fig. 4. The relative error in the RHF monotonically grows with r_s, so that even at $r_s\approx 5$, the correlation energy is some 10% of the exact energy. The UHF relative error is, however, nonmonotonic. It reaches a maximum of ≈9% ar $r_s\approx 8$, and for large r_s tends to a value of ≈4%. This indicates that the UHF solutions do best at the two limits, small and large r_s, and poorly in the intermediate r_s regime.

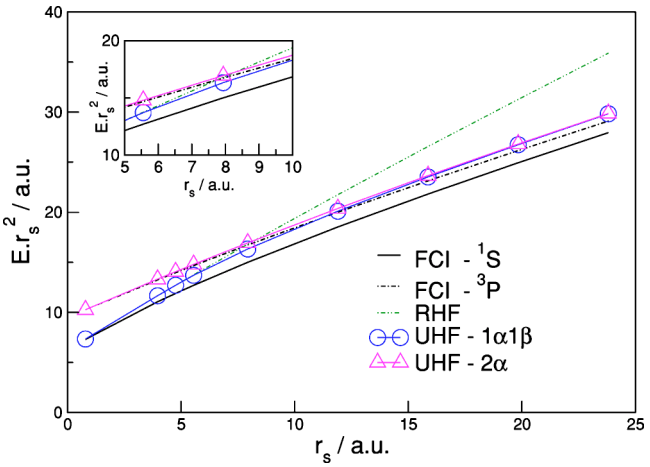

FIG. 3. The scaled energy of the two-electron system for the CI, RHF, and UHF studies as a function of r_s. The inset to this figure highlights the Coulson–Fischer transition (occurring at $r_s\approx 6$) and the subsequent breaking of the degeneracy of the UHF ($m_s=0$) and RHF energies.

TABLE IV. Convergence of the UHF energy, as a function of μ_{max} and l_{max} for the two-electron system for several different R.

Radius	μ_{max}	l_{max}	$m_s=0$	$m_s=1$
1	3	1	11.641 749 013	16.284 518 26
		2	11.641 749 013	16.281 956 26
		3	11.641 749 013	16.281 956 07
		4	11.641 749 013	16.281 956 05
5	3	1	0.739 764 754	0.847 889 736
		2	0.739 764 754	0.845 314 214
		3	0.739 764 754	0.845 308 980
		4	0.739 764 754	0.845 308 611
20	3	1	0.096 127 832	0.096 279 716
		2	0.093 380 670	0.093 943 058
		3	0.093 329 833	0.093 859 098
		4	0.093 329 751	0.093 858 859

We also compare the SCF densities with those arising from the CI solutions. We consider the RHF and low-spin UHF state along with the LDA density for four different sized spheres (Fig. 5). For $R=1$ (a) all solutions give comparable results, with both HF and LDA densities being faithful representations of the exact result. As R increases, the lack of the appropriate α-β correlation in the RHF approach is clear, with the density being strongly peaked at the origin

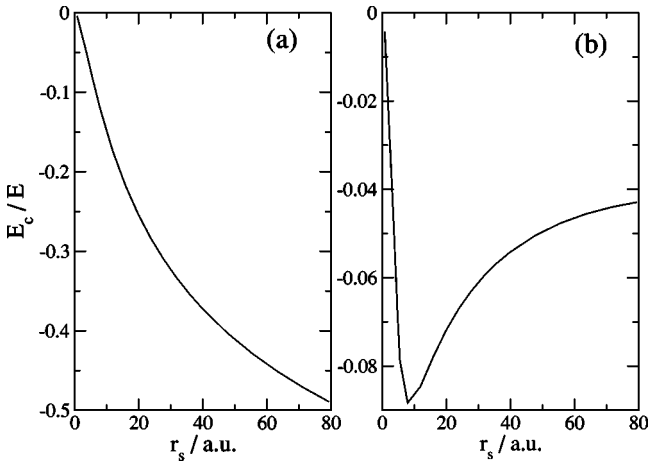

FIG. 4. The function E_c/E for the RHF (a) and UHF (b) solutions.

even though for $R=10$ (b) the exact solution is within a Wigner molecule state (showing a minimum at the origin). (All methods show this state forming with the crossover radii being $R_c^{\mathrm{RHF}}\approx 13$, $R_c^{\mathrm{UHF}}\approx R_c^{\mathrm{PZ}}\approx 8$, and $R_c^{\mathrm{CI}}\approx 7$. For further increases in R, the LDA density is seen to behave poorly; it greatly exaggerates the localization of the density towards the sphere boundary.) This behavior could be due to the incorrect self-interaction behavior of the local density functionals. Very similar behavior has been found by Jung *et al.*, who found that the commonly used generalized gradient approximations (GGA) and meta-GGAs do poorly at reproducing the shape of the density at the center of the sphere. By contrast the UHF densities, which are correctly self-interaction-free, are comparatively good: the agreement with the exact behavior is excellent at small and large R, while exhibiting marked deviations for intermediate R.

To obtain further insight into this, it is instructive to perform a population analysis on the low-spin UHF and ^1S CI wave function. In the former case we have used the density matrix $P_{\mu\nu}$ and note that $p_l=\Sigma_{\mu\mu\in l}P_{\mu\mu}$; p_l giving the total population of the lth angular momentum component in the wave function. This provides a convenient measure of the amount of $s,p,d,\ldots$, character in the wave function. To perform a similar analysis upon the CI wave function required computation of the natural orbitals from the CI first-order density matrix and then an angular momentum decomposition as described. The results of the population analysis are shown in Fig. 6. The wave function has pure s character up to $r_s\approx 4$, the subsequent onset of the spatial separation of the two spin components, which is reflected in the increased p and d character of the UHF solutions preceeds the Coulson–Fischer transition, occuring at $r_s\approx 6$. This is a reasonable imitation of the behavior of the CI wave function, which exhibits smooth behavior. With increasing R, the ^1S wave function gradually decreases in s character, while smoothly increasing p, and to a lesser extent the d, character (the latter is too small to plot). From the viewpoint of the UHF wave function, the markedly growing p character which occurs immediately after the Coulson–Fischer transition, leads to

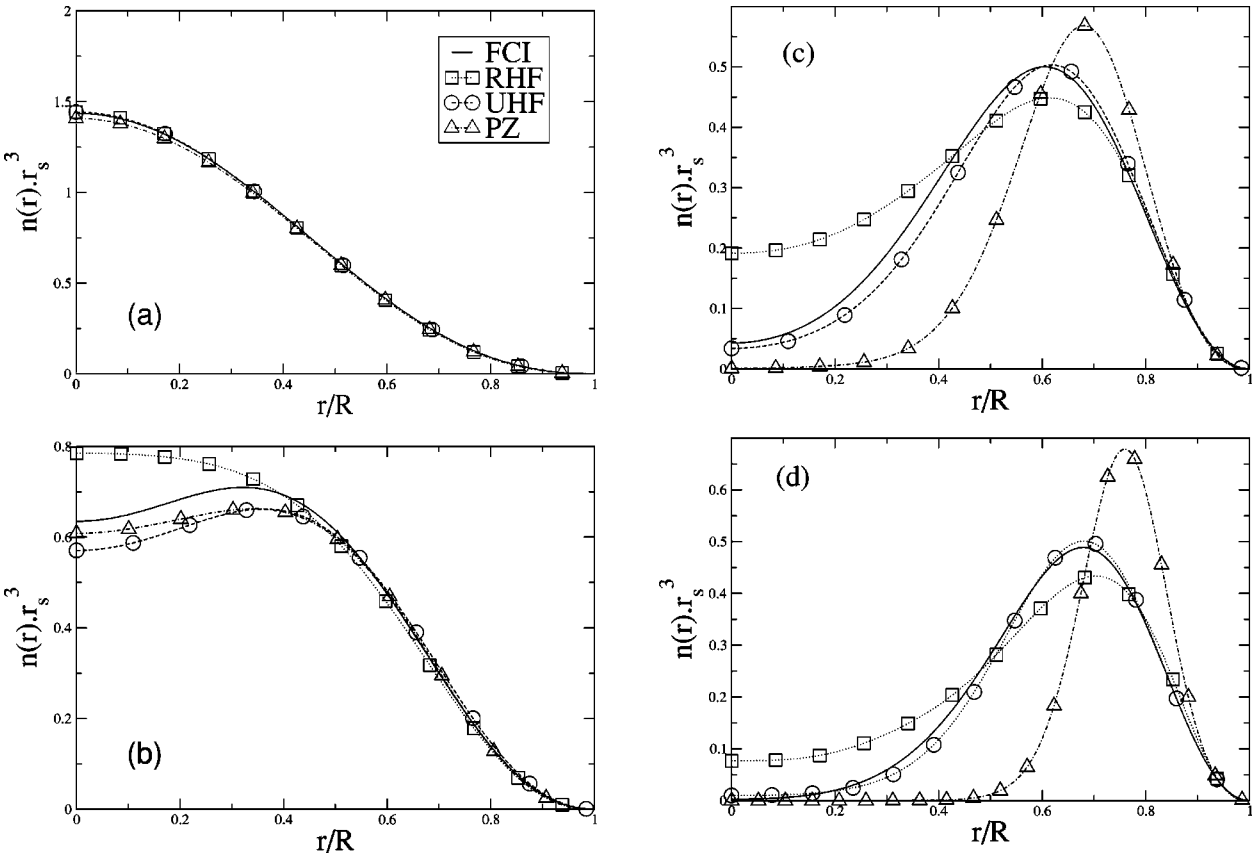

FIG. 5. Showing the ground state electron density at the RHF, UHF, LDA, and CI levels of theory for two electrons confined within a sphere. We consider here (a) $R=1$, (b) $R=10$, (c) $R=50$, and (d) $R=100$. We note the success of the UHF theory at essentially reproducing the exact result for large R.

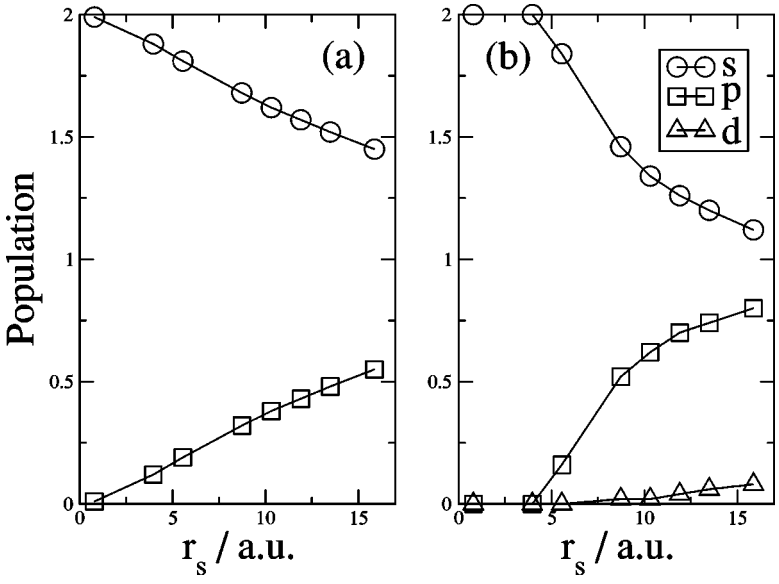

FIG. 6. Population analysis of the CI wave function (a) and the low-spin UHF wave function (b). The degeneracy of the UHF and RHF solutions is seen to persist until $R \sim 5$. In general, the UHF wave function is able to mimic the CI wave function successfully for a wide range of R.

UHF densities which exaggerate the Wigner-molecule density profile, this being most noticeable at the onset of the Wigner-molecule formation [e.g., Fig. 5(b)].

V. CONCLUSION

We have computed the RHF and UHF solutions of the model problem of two-interacting electrons confined to a sphere. These solutions have been computed to a high accuracy and calculations were performed on confined atomic systems to benchmark our implementation. We find that until $r_s \approx 6$ the restricted and unrestricted solutions are degenerate. Beyond this, the unrestricted energy is seen to become lower. Furthermore, the unrestricted energy and electron density compare favorably with the configuration interaction study in the small r_s and large r_s limits. A Coulson–Fischer transition occurs at an r_s close to that at which the CI density acquires a minimum at the sphere center; where this observance of a minimum in the density at the origin is identified as the onset of formation of a Wigner molecule. In this regime, however, the HF densities and energies are not quantitatively accurate when compared to the CI ones. Furthermore, to highlight this failure, we have computed the exact correlation energy, defined with respect to the UHF and RHF states over a range of r_s. The error in the correlation energy is seen to be greatest in the crossover regime from "liquid" to "Wigner state." Thus, while being reasonably accurate at both high and low densities, the failure of the UHF solution within this intermediate regime is clear; further evidence that care be taken when modeling these few-electron systems using HF theory.

ACKNOWLEDGMENT

The authors wish to thank J. Jung for helpful discussions and providing them with a preprint of Ref. 26.

[1] N. R. Kestner and O. Sinanoğlu, Phys. Rev. **128**, 2687 (1962).
[2] M. Taut, Phys. Rev. A **48**, 3561 (1993).
[3] P. M. Laufer and J. B. Krieger, Phys. Rev. A **33**, 1480 (1986).
[4] C. Filippi, C. J. Umrigar, and M. Taut, J. Chem. Phys. **100**, 1290 (1993).
[5] S. Kais, D. R. Herschbach, N. C. Handy, C. W. Murray, and G. J. Laming, J. Chem. Phys. **99**, 417 (1993).
[6] K. Burke, F. G. Cruz, and K.-C. Lam, Int. J. Quantum Chem. **70**, 583 (1998).
[7] D. Frydel, W. M. Terilla, and K. Burke, J. Chem. Phys. **112**, 5292 (2000).
[8] D. C. Thompson and A. Alavi, Phys. Rev. B **66**, 235118 (2002).
[9] J. Jung and J. E. Alvarellos, J. Chem. Phys. **118**, 10825 (2003).
[10] E. Wigner, Phys. Rev. **46**, 1002 (1931).
[11] C. C. J. Roothaan, Rev. Mod. Phys. **23**, 69 (1951).
[12] W. H. Press, B. P. Flannery, S. A. Teukolksy, and W. T. Vetterling, *Numerical Recipes in Fortran*, 2nd ed. (Cambridge University Press, Cambridge, 1992).
[13] J. A. Pople and R. K. Nesbet, J. Chem. Phys. **22**, 571 (1954).
[14] We used the real-symmetric diagonalization routine DSYEVX of the LAPACK package.
[15] A. Szabo and N. S. Ostlund, *Modern Quantum Chemistry* (McGraw-Hill, Mineola, NY, 1989).
[16] L. E. Brus, J. Chem. Phys. **80**, 4403 (1984).
[17] G. M. Harris, J. E. Roberts, and J. G. Trulio, Phys. Rev. **119**, 1832 (1960).
[18] A. Michels, J. De Boer, and A. Bijl, Physica (Amsterdam) **4**, 981 (1937).
[19] C. A. Ten Seldam and S. R. De Groot, Physica (Amsterdam) **10**, 891 (1952).
[20] C. A. Ten Seldam and S. R. De Groot, Physica (Amsterdam) **18**, 905 (1952).
[21] D. S. Krähmer, W. P. Schleich, and V. A. Yakovlev, J. Phys. A **31**, 4493 (1998).
[22] J. L. Marín and S. A. Cruz, J. Phys. B **25**, 4365 (1992).
[23] S. A. Cruz and J. Soullard, Int. J. Quantum Chem. **83**, 271 (2001).
[24] G. N. Watson, *A Treatise on the Theory of Bessel Functions* (Cambridge University Press, Cambridge, 1996).
[25] J. P. Perdew and A. Zunger, Phys. Rev. B **23**, 5048 (1981).
[26] J. Jung, P. García-González, J. E. Alvarellos, and R. W. Godby, Phys. Rev. A **69**, 052501 (2004).
[27] C. A. Coulson and I. Fischer, Philos. Mag. **40**, 386 (1949).
[28] N. C. Handy and A. J. Cohen, Mol. Phys. **99**, 403 (2001).
[29] B. Y. Tong and L. J. Sham, Phys. Rev. **114**, 1 (1966).